Review article **Open Access**

Yachao Liu, Yougang Ke, Hailu Luo* and Shuangchun Wen

Photonic spin Hall effect in metasurfaces: a brief review

DOI 10.1515/nanoph-2015-0155
Received December 18, 2015; revised March 23, 2016; accepted March 25, 2016

Abstract: The photonic spin Hall effect (SHE) originates from the interplay between the photon-spin (polarization) and the trajectory (extrinsic orbital angular momentum) of light, i.e. the spin-orbit interaction. Metasurfaces, metamaterials with a reduced dimensionality, exhibit exceptional abilities for controlling the spin-orbit interaction and thereby manipulating the photonic SHE. Spin-redirection phase and Pancharatnam-Berry phase are the manifestations of spin-orbit interaction. The former is related to the evolution of the propagation direction and the latter to the manipulation with polarization state. Two distinct forms of splitting based on these two types of geometric phases can be induced by the photonic SHE in metasurfaces: the spin-dependent splitting in position space and in momentum space. The introduction of Pacharatnam-Berry phases, through space-variant polarization manipulations with metasurfaces, enables new approaches for fabricating the spin-Hall devices. Here, we present a short review of photonic SHE in metasurfaces and outline the opportunities in spin photonics.

Keywords: photonic spin Hall effect; metasurfaces; spin-orbit interaction; geometric phase; spin-Hall devices.

1 Introduction

Photonic spin Hall effect (SHE) refers to the splitting of opposite spin photons perpendicular to the incident plane of light beam, which is the result of the spin-orbit interaction in light propagation [1, 2]. This effect can be regarded as a photonic counterpart of the electronic SHE, where the spin electrons are accumulated at the opposite sides of an electron flow [3–6]. Spin is the intrinsic angular momentum of element particles. For photons, the opposite spin angular momenta correspond to the right and left circular polarizations of light beam. And the direction of wave vector is closely associated with the orbital angular momentum. Thus, the photonic SHE builds a bridge between the polarization and orbital angular momentum of light. By introducing a controllable photonic SHE in light-matter interaction, the spin and orbital freedoms can both be manipulated.

In the traditional cases, the spin-dependent splitting created by the photonic SHE in light deflection is limited to a fraction of one wavelength. This is due to the fact that the spin-orbit interaction is very weak. Extremely precise metrology is required for the detection of such phenomenon. Quantum weak measurement first proposed by Aharonov, Albert, and Vaidman in 1988, which was based on preselection and postselection states, is a promising method for measuring the tiny perturbations in quantum system [7]. Hosten and Kwiat successfully employed the quantum weak measurement technology to amplify and detect the photonic SHE occurring at an air-glass interface in 2008 [8]. And then, with the sensitive relationship between the photonic SHE and the physical parameters of the interface, a series of works based on the quantum weak measurement are dedicated to the measurement of tiny physical parameters [9–14].

Another effort is to enhance the photonic SHE by introducing a stronger or enlarged spin-orbit interaction. The multiple reflections of light in a glass cylinder can efficiently enhance the photonic SHE by increasing the distance of interaction [15]. Moreover, the photonic SHE can also be enhanced in some particular situations [16–20]. Nevertheless, there is still a long distance to arbitrarily manipulate the photonic SHE. The development of metasurfaces, metamaterials with a reduced dimensionality [21], provides a possible solution to this problem [22].

Metasurfaces have demonstrated exceptional abilities in controlling the light flow compared with conventional interfaces between two materials and that it enables new

***Corresponding author: Hailu Luo,** Laboratory for Spin Photonics, School of Physics and Electronics, Hunan University, Changsha 410082, China, e-mail: hailuluo@hnu.edu.cn
Yachao Liu, Yougang Ke and Shuangchun Wen: Laboratory for Spin Photonics, School of Physics and Electronics, Hunan University, Changsha 410082, China

physics and phenomena that are unprecedented in their 3D counterparts [21–29]. By artificially defining their building blocks, such as the material, geometry, orientation, and arrangement, the spatial and spectral dispersions of the dielectric and magnetic properties can be managed in the metasurfaces [30–37]. Yin et al. applied metasurface to obtain a giant photonic SHE in 2013 [22]. The designed rapid phase variation along transverse direction leads to the deflection of light, while a geometric polarization rotation is implemented in this process to maintain the polarization transverse to its new propagation direction. As the result of spin-orbit interaction, the geometric polarization rotation leads to the spin-dependent splitting of light.

However, a more direct way can be introduced to manipulate the spin-orbit interaction in metasurfaces, which is to tailor the polarization in the beam cross-section [24–26, 38–40]. In this paper, we will review the observable photonic SHE generated by introducing a designed spin-orbit interaction through the metasurfaces. Particularly, we will focus on the photonic SHE caused by the polarization tailoring and the different manifestations. In Section 2, a brief introduction is made to the spin-orbit interaction, the geometric phases, and the realization of metasurfaces based on subwavelength structure, which are the basic principles for manipulating the photonic SHE in metasurfaces. In Section 3, the recent advances of observable photonic SHE in metasurfaces are divided into two classes, with splitting in position space and in momentum space. In Section 4, we focus on the spin-Hall devices, a class of optical metasurfaces with multifunctionality and infinitesimal thickness. In Section 5, perspectives of the future opportunities in the research of photonic SHE and a brief conclusion are given.

2 Manipulation of spin-orbit interaction with metasurfaces

2.1 Spin-orbit interaction

It is well known that light carries both energy and momentum. The momentum of light can be divided into linear and angular contributions [41]. In paraxial approximation, the angular momentum of light has a spin part associated with circular polarizations [42] and an orbital part associated with the direction of wave vector or phase front [43, 44]. Spin-orbit interaction describes the mutual influence between the spin and orbit angular momenta of light [41, 45–49]. Generally, the trajectory of beam is associated with the external part of the orbit angular momentum. As a result of spin-orbit interaction, the variation of trajectory is always accompanied with the transverse spin-dependent deflection, namely, the photonic SHE. In experiments, this effect is so weak that a precise measurement technique is required to observe it [7] or it can be observed under an enhanced interaction led by the multireflection in an isotropic material [15]. Additionally, the helical structure of optical wavefront around the beam axis (i.e. the optical vortex located at the beam axis) is associated with another internal form of orbital angular momentum [50, 51]. With the rapid development in generating and manipulating the optical vortex beams, the interaction between spin and this internal orbital angular momentum gathers more and more interests in recent years.

Geometric phases are the performances of spin and orbit angular momentum interaction, which are different from the traditional dynamic phases as they are not integrated as the increase of optical propagation length [52, 53]. It is the change of geometric properties of beam which contributes a phase difference to the light [51–58]. Polarization and spatial propagation are the major geometric properties of beam. Therefore, two kinds of geometric phases are found in the early researches in succession [59, 60]. The first class is spin-redirection phase, which was found by Rytov in 1938 [61] and then developed by Vladimirskii [62] and Berry [63]. The variation of propagation direction in SO(3) space (position space) will lead to the phase difference in wave function. The other kind of geometric phase is dubbed as Pancharatnam-Berry (PB) phase [64–67], which is named after its finders, Pancharatnam and Berry. Differently, it is related to the polarization variation in SU(2) space, namely, the polarization space. Both the spin-redirection and PB phases are the manifestations of spin-orbit interaction.

Spin and orbit angular momenta are the intrinsic freedoms of light, which can basically extend the capacity of information encoding and provide a brand-new way to manipulate light. Spin-orbit interaction relates them and gives a feasible approach to utilize them. Efforts in this topic have shown great potentials in communication, particle manipulation, optical design, and optical computation. Geometric phases are the quantitative representations of spin-orbit interaction and are the reasons of spin-dependent behaviors of light in propagation. Therefore, simple descriptions of geometric phases are firstly presented in the following.

2.2 Spin-redirection phase

Berry phase is well known as a phase difference acquired when a quantum system described by a Hamiltonian is

subjected to a cycle of time-dependent adiabatic parameter, which is first pointed out by Berry in 1984 [63]. However, the findings about phase difference in optical systems were presented long before it [61, 62]. Propagation and polarization are the vector properties of a light beam. For the first category, the variation of propagation direction contributes to the spin-redirection phase. In particular, it induces an additional term in the equations of motion (ray equations) which describes a polarization-dependent shift of the beam trajectory.

Figure 1 shows the evolution of a light beam. Triad vector (***x***, ***y***, ***z***) is the laboratory coordinate frame, where the momentum direction of light beam ***t*** is recorded. An attached coordinated frame (***t***, ***v***, ***w***) is applied to describe the transverse properties. As shown, the polarization state ***e*** will rotate with the evolution of light beam. This effect can also be represented in a unit sphere, where each point on the surface stands in a unique direction in position space. The evolution trajectory of momentum direction is depicted in Figure 2. For a loop trajectory, marked by a green dash line in the sphere, the polarization state rotated from ***e*** to ***e′***. Under the spin-orbit interaction, polarization rotation in the beam transverse section will lead to a back-action on the orbital angular momentum of light, namely, the spin-redirection phase. This geometric phase is different for the spectra components in a light beam, which will finally lead to the transverse shift of light beam.

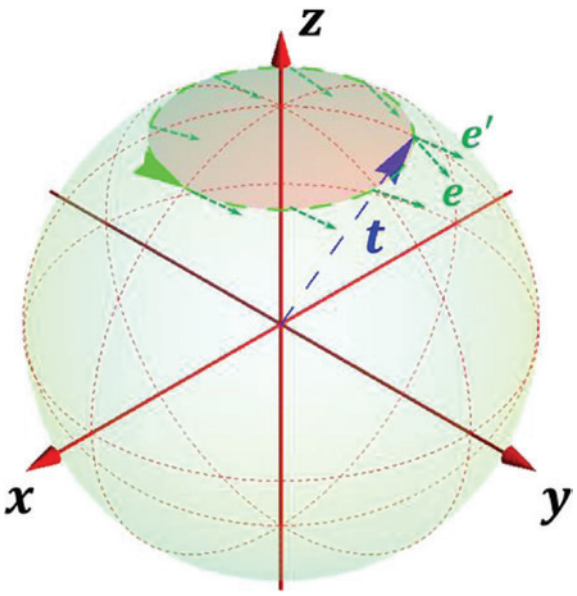

Figure 2: The parallel transport of the polarization vector ***e***⊥***t*** on the unit ***t***-sphere in momentum space. For a loop trajectory, the polarization states rotate from ***e*** to state ***e′***.

2.3 Pancharatnam-Berry phase

The PB phase is associated with the polarization variation of light. To trace out the variation, Poincaré sphere is the most valid representation. The polarization of light can be characterized by the Stokes parameters (S_0, S_1, S_2, S_3) in general [68]. For a totally polarized beam, these parameters will fulfill the relationship $S_0^2=S_1^2+S_2^2+S_3^2$, where $S_0=1$ as the field is normalized. Thus, a unit sphere can be constructed based on the coordinates ($\boldsymbol{S_1}$, $\boldsymbol{S_2}$, $\boldsymbol{S_3}$); each point on the surface of Poincaré sphere will be solely related

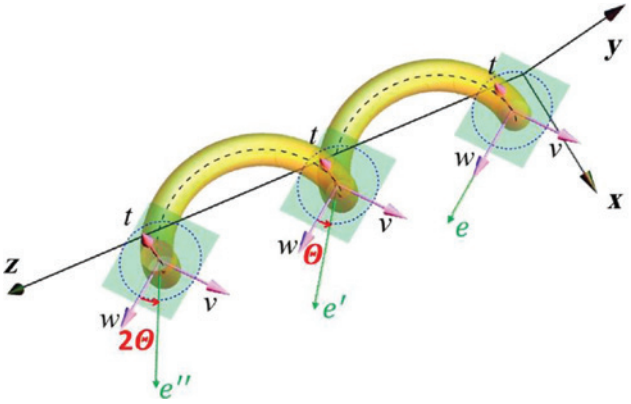

Figure 1: The polarization evolves along a twisted ray trajectory, obeying the parallel transport law. The wave polarization is measured in a coordinate frame with basic vectors (***t***, ***v***, ***w***) accompanying the ray, where ***t***=***p***/*p* is the tangent to the trajectory.

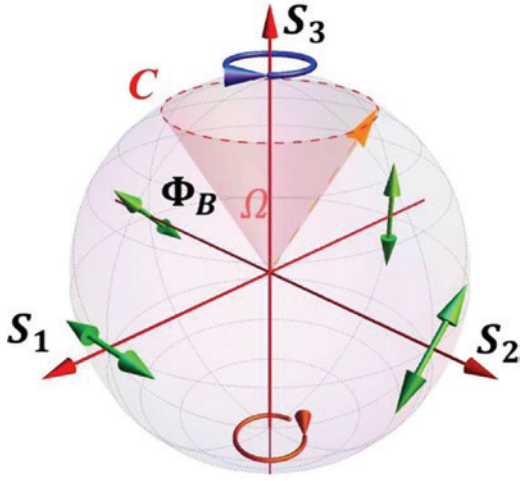

Figure 3: The polarization evolution is represented by the precession of the Stokes vector ($\boldsymbol{S_1}$, $\boldsymbol{S_2}$, $\boldsymbol{S_3}$) on the Poincaré sphere about the $\boldsymbol{S_3}$ axis. The Stokes parameters are applied to characterize the polarizations of light; for a polarized beam, they hold relationship $\boldsymbol{S_1}^2+\boldsymbol{S_2}^2+\boldsymbol{S_3}^2=1$. Poles of this unit sphere represent circular polarizations, the equatorial points represent the linear polarizations, and the internal points are elliptical polarizations. The polarization states on the coordinate axes are marked by arrow lines.

to a general polarization state. Figure 3 shows a general Poincaré sphere. The poles represent circular polarizations; equatorial points are linear polarizations; and the other points between the poles and equator are elliptical polarizations. Four linear polarizations are marked on the equator of Figure 3, and the poles are assigned with opposite circular polarizations (σ=±1). It is clear that the diametrically opposite points on Poincaré sphere represent the orthogonal polarizations.

For a cyclical evolution on the Poincaré sphere, just for example as the route C described in Figure 3, the PB phase Φ_B included can be deduced as the half of solid angle Ω enclosed by the route on the surface. Therefore, it is a feasible approach to manipulate the phase of light by controlling polarization, which is currently attracting growing attention.

Polarization is the fundamental feature of electromagnetic waves. The studies of polarization have been extended to a wide category in the past decades. However, Poincaré sphere is still limited to the representation of most simple and primary homogeneous plane polarization states. To adjust the general Poincaré sphere to more complicated situations, higher-order Poincaré sphere [69, 70], orbital Poincaré sphere [71], and hybrid order Poincaré sphere [72] are developed recently. The transverse phase structure of light beam is associated with the internal orbital angular momentum of light, which provides an additional degree of freedom for beam manipulation and data encoding. Thus, the orbital angular momentum carrying beams also requires a prominent geometrical representation. Orbital Poincaré sphere is the analogy of general polarization Poincaré sphere in phase space. Cylindrical vector (CV) beams are light beams of which the polarization states are arranged with cylindrical symmetry in the beam cross section, which is the higher-order solution of Maxwell's vector wave equation. Many unique properties originating from the special intrinsic symmetry of CV beams have distinguished them from the general optical beams with homogeneous polarization. Similar to Poincaré sphere, higher-order Poincaré sphere is lately developed to describe the CV beams.

Figure 4 shows the representation of higher-order Poincaré sphere (l=σ=1), and each point (θ, ϕ) along the surface describes a higher-order polarization state, where the poles represent circularly polarized optical vortexes with orthogonal chiralities and opposite topological charges; the points on equator represent polarization states that are linearly polarized and azimuthally arranged, and the intermediate points between the poles and equator represent elliptically polarized vector states. For more general cases, the higher-order Poincaré sphere

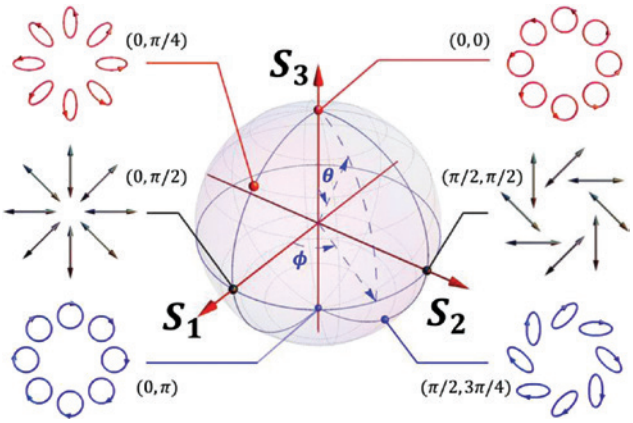

Figure 4: Higher-order Poincaré sphere (l=1): the poles (θ=0, π) represent orthogonal circular polarizations with different optical vortex (l=±1). Equatorial points (θ=π/2) represent generalized cylindrical vector beams; (ϕ=0; θ=π/2) and (ϕ=π; θ=π/2) represent radial and azimuthal vector beams, respectively; (ϕ=π/2; θ=π/2) and (ϕ=3π/4; θ=π/2) represent spiral polarizations. Intermediate points between the poles and equator represent elliptically polarized cylindrical vector beams.

will be reduced to the standard Poincaré sphere when l=0. Moreover, the handedness of optical vortex and circular polarization at each pole can be adjusted in the same or opposite senses. As a consequence, the polarization state collection in each order (l) can be enclosed by two spheres with opposite σ. In this geometric representation, higher-order PB phase is demonstrated by cyclic transformation of the CV beams on the higher-order Poincaré sphere. The resulting geometrical phase is then given by [69]

$$\phi_g \propto (l+\sigma)\Omega/2, \tag{1}$$

where Ω is the solid angle subtended by the area enclosed in the evolving route; l and σ are the topological charge and spin assigned to the sphere, respectively.

From the three kinds of Poincaré spheres mentioned above, the orthogonal eigenstates of the whole state-space are settled at the opposite poles of the sphere. For the standard Poincaré sphere, poles are marked with the opposite spin states σ=±1; for the orbital Poincaré sphere, poles are assigned with the contrary topological charges ±l; and for the higher-order Poincaré sphere, poles are ruled with both the opposite spin and topological charges ±l, σ=±1. All in all, the states on the poles of sphere are orthogonal but in a value, i.e. the same order. Then, what will be the evolution of phase and polarization states between different orders? To describe this situation and find out the PB phase involved, a hybrid-order Poincaré sphere is recently developed. Figure 5 describes the representation of a hybrid-order Poincaré sphere [72]. It is

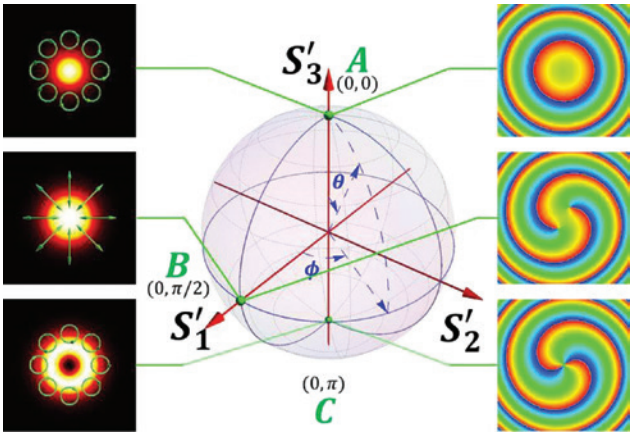

Figure 5: Schematic illustration for the evolution of phase and polarization states on hybrid-order Poincaré sphere. Insets in the right row show the phases of points A, B, and C, respectively. Insets in the left row show the polarization states of the three points. Here, we assume the north pole with state σ=±1 and l=0, while the south pole is with σ=-1 and l=1.

based on the finding that the representation of the polarization states in inhomogeneous anisotropic media has a similar expression of polarization states on the higher-order Poincaré sphere with only the orbital states being different. Therefore, the polarization and phase evolution in inhomogeneous anisotropic media with special geometry can be conveniently described by the evolution of states along the geodesic lines on the hybrid-order Poincaré sphere. The PB phase associated within this process are discussed as well

$$\phi_g \propto -\frac{l-(m+2\sigma)}{4}\Omega, \tag{2}$$

where l and m are the topological charges of the north and south poles, respectively; σ is the primary spin state; and Ω represents the solid angle faced by the encompassed area.

2.4 Metasurfaces based on subwavelength structure

The manipulation of wavefront is generally realized by introducing the changes of phase and polarization of light [73, 74]. Traditional optical devices are based on the reflection, refraction, or diffraction effects in media to accumulate these variations for light manipulations [75–77]. Thus, the volume size of traditional devices is limited by the propagation effects. To expand functionality and miniaturize the optical elements, metasurfaces with a reduced dimensionality are developed in recent years, which breaks the restriction of light propagation by introducing feature variations in the scale of operating wavelength [21, 27, 29]. Additionally, the metasurfaces made of arrays of scatters can be arranged with a spatially varied geometry (size, orientation, and shape). Hence, the spatially varied responses of the beam wavefront can be artificially managed.

Two kinds of scatters are applied in the up-to-date phase designing of metasurfaces based on subwavelength structure. This first kind uses the dispersion of scatters to add abrupt phase changes in light propagation [22, 78–82]. A canonical example is the V-shape antennas as shown in Figure 6A [23, 30, 83–87]. When a light beam impinges on a metallic antenna, the light wave will couple with the surface wave and the electron oscillation in the antennas, namely, with the surface plasmons. The phase difference induced in the propagation wave of metasurface is a result of strong interaction between light and the local surface plasmon polaritons (SPPs). When metallic

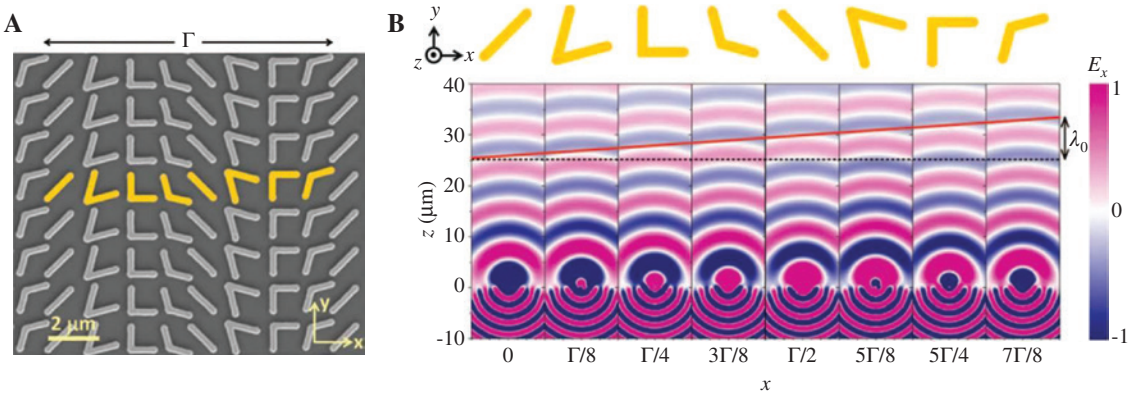

Figure 6: (A) The SEM image of metasurface based on the V-shape antennas. (B) The scattered electric field corresponds to the individual antennas in the left picture. Adapted from Ref. [23].

antenna geometry satisfies the resonance requirement, the incident field will keep in phase with the excited surface current. The surface current will lead or lag the incident field. As with the accordance of surface current and the scattered field, the phase of scattered field can be controlled by altering the geometry of metallic scatters, as the example in Figure 6B. Additionally, V-shape antennas allow one to design the amplitude, phase, and polarization state of the scattered light, since two orthogonal modes can be excited by the incident field. According to Babinet's principle, the V-shape slits milled in a thin metallic film can also be applied to manipulate the features of light [88].

Another kind of scatter introduces phase change by controlling the local polarization states of the light beam [38, 57, 58, 89–98]. As introduced in the last section, the polarization evolution will lead to phase change in waves. By locally tailoring the evolving routes of polarization, a desired phase distribution can be expected in the scattered field. The most used polarization devices in traditional optics is the polarizer and waveplate. The former one is a filter which chooses a specific polarization component from the incident field, while the last one can convert the polarized beam to a certain polarization state. By designing the geometry of scatters, both the function of polarizer and waveplate can be realized in the subwavelength scale, as the examples shown in Figure 7. The rectangular apertures milled in a metallic thin film functions like a miniature polarizer. And the polarization of transmitted light is primarily perpendicular to the long axis of aperture. Thus, the metasurface shown in Figure 7A will lead to the phase variation around the center axis, namely, an optical vortex as shown in Figure 7B [93]. Figure 7C and D exhibit the structure and experimental results of another optical vortex generator, which is based on the rectangular antennas serving as miniature waveplates [57]. Therefore, the continuous tailoring of wavefront is feasible by engineering the polarization.

The dielectric metasurfaces constructed by continuous or quantized subwavelength gratings can also be applied to modulate the polarization states of the light beam [58, 90]. When the period of grating is much smaller than the wavelength of incident beam, only the zeroth order is propagating, while the others are suppressed. Homogeneous gratings are operating as a uniaxial crystal with its optical axes parallel and perpendicular to the gratings. It means that the electric fields oscillating along or orthogonally across the grating will obtain the different

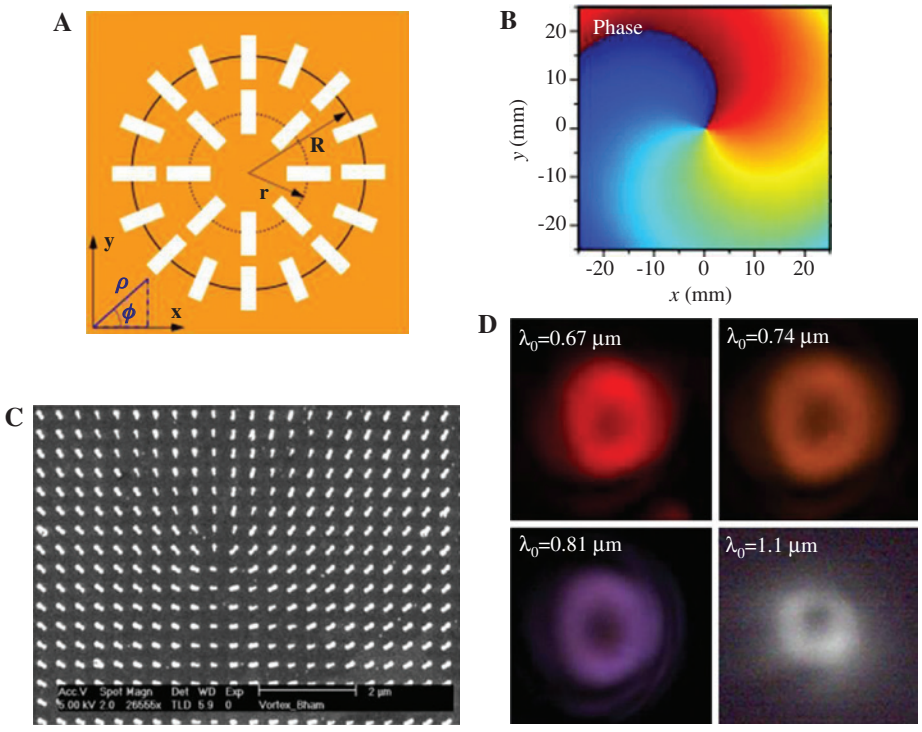

Figure 7: The metasurfaces based on the PB phase scatters. (A) and (B) The schematic and phase distribution of a rectangular apertures comprised metasurface, which serves as a vortex beam generator. Each rectangular aperture can be regarded as a polarizer working at a fixed wavelength. (C) and (D) The SEM image and intensity distribution obtained from a dipolar antenna array. The antennas have the same geometry but varied orientations. Each antenna can be treated as a nano-waveplate. Adapted from Refs. [57, 93].

phase shifts. Therefore, it leads to the so-called form birefringence, contrasting to the birefringence originating from the anisotropy of oriented molecules [91]. By designing a spatially varying subwavelength grating, the polarization can be manipulated in each exact location. Thus, a metasurface with sophisticated function can be realized. The quantization of subwavelength grating will sufficiently alleviate the difficulty in designing and fabricating [58, 90].

3 Photonic spin Hall effect

Hall effect refers to the transverse voltage difference generated when an electric conductor is placed under the perpendicular magnetic field, because of the transverse transportation of electrons [99]. Spin angular momentum is an intrinsic property of elementary particles; for example, electrons have spin with $\pm 1/2\hbar$, where $\hbar$ is the reduced Plank constant. Similar to the Hall effect, the spin of electron will also accumulate at the boundary of an electric-current-carrying conductor, which is the SHE in an electric system [100–103]. Photons are also assigned with spin angular momentum equal to $\sigma\hbar$, where $\sigma=\pm 1$. Therefore, the SHE is also expected in the optical system [1, 2, 104]. Researches in SHE of electrons have been done for decades; however, the photonic SHE has been observed just in recent years [8].

The spin accumulation in an optical system is also the result of spin-orbit interaction. However, the limited amount of angular momentum that a photon carries makes it a considerable challenge to directly observe this effect. Two different approaches are proposed to solve the problem. The first one is to find an extremely precise detection method. Quantum weak measurement is a solution that can be applied to observe the photonic SHE, and more importantly, it provides a feasible way to determine the physical parameters with photonic SHE [8–12]. Therefore, a series of applications are developed. The second way is to enhance the spin-orbit interaction involved in the process of spin angular momentum accumulation [22, 26, 38]. In this way, the photonic SHE is divided into two categories: the splitting based on the spin-redirection phase lead by the spin-orbit interaction will take place at position space, and the splitting that resulted from PB phase will occur at momentum space. Those two kinds of photonic SHE can both be modulated by using the metasurfaces. Thus, we make a detailed introduction of these two kinds of splitting in the following. Additionally, the photonic SHE may also be observed in some special situations, where the splitting of light is independent of the light-matter interaction [105–107].

3.1 Spin-dependent splitting in position space

As mentioned above, the variation of propagation orientation will lead to the phase change in wave beam, which is the spin-redirection phase [59, 62, 63]. For different angular spectral components, the introduced phase changes are different as well. Therefore, a phase gradient is presented between the different spectral components. The phase gradient of angular spectral component will lead to a spin-dependent shift in position space,

$$\Delta \boldsymbol{r}=\nabla \boldsymbol{\Phi}_{\boldsymbol{G}}(k_x, k_y), \tag{3}$$

where $\nabla \boldsymbol{\Phi}_{\boldsymbol{G}}(k_x, k_y)$ is the gradient of geometric phase and is a function of transverse wave vectors (k_x, k_y). The z-direction is assumed as the direction of normal incidence, where xz plane is the incident plane of light. Thus, the spin-dependent splitting in y-direction is the expected photonic SHE lead by spin-redirection geometrical phase.

The magnitude of induced spin-redirection phase can be found in the reflection or refraction equation of light, where the component of k_y is the reason for spin-dependent splitting in y-direction, which is in the following form:

$$\boldsymbol{\Phi}_{\boldsymbol{G}}(k_y)=\sigma k_y \delta, \tag{4}$$

where σ refers to spin of incident light, $\delta \propto \cot\theta_i/k_0$, θ_i is the incident angle, and k_0 is the wave number in a vacuum. The magnitude of δ is related to the physical parameter of interface [108]. For example, the thickness of interface can be modulated to enhance the effect. Bliokh et al. proposed an efficient way to directly observe the photonic SHE by guiding the light beam in a glass cylinder as shown in Figure 8. The long propagation route in glass cylinder amplifies the spin-dependent splitting [15].

Metasurfaces can also be applied to manipulate the spin-dependent splitting in position space by enhancing the spin-orbit interaction [22]. By designing a two-dimensional (2D) electromagnetic nanostructure as shown in Figure 9A, an in-plane phase retardation is introduced in wavelength scale at the beam transverse section. The phase retardation makes the anomalous scattering of passing light, which therefore dramatically changes the related physical parameters of this artificial interface. Thus, the photonic SHE can be directly observed in the experiment. Figure 9 shows the experimental apparatus

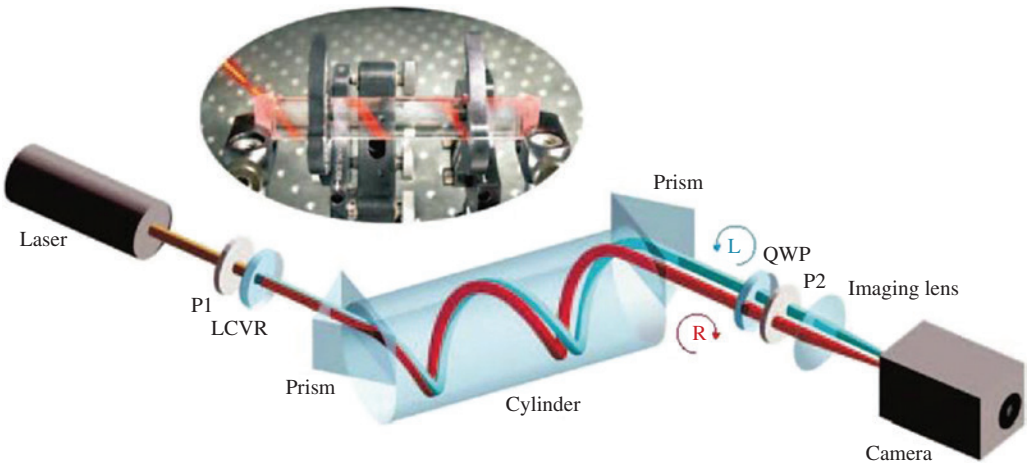

Figure 8: A laser beam enters the glass cylinder at a grazing angle through the input prism, coils along the cylinder surface, and leaves it by means of the output prism. The liquid-crystal variable retarder (LCVR) is used for generating and switching between the circularly polarizations, whereas the quarter-wave plate (QWP) and polarizer P2 are intended for measurement of the Stokes parameters. The inset shows a real picture of the spiral light beam inside the cylinder. Adapted from Ref. [15].

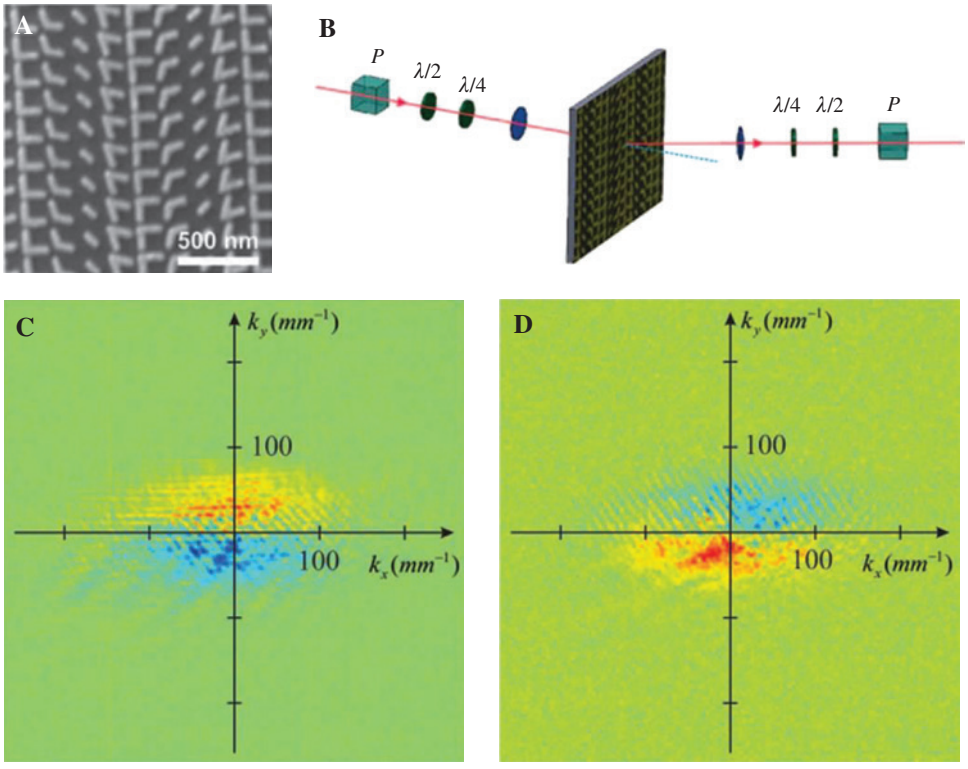

Figure 9: The photonic SHE related to spin redirection phase is directly observed by introducing an ultrathin metasurface. (A) The scanning electron microscope image of metasurface designed by arranging the V-shape antennas in *x*-direction. (B) The schematic illustration of the observing setup. (C) and (D) are the measured S_3 when polarization of incident beam is changed from linear polarization in *x* direction to *y* direction. Adapted from Ref. [22].

and observed S_3 results. This work shows the possibility of controlling the photonic SHE by designing the metasurfaces, which not only provides a novel application of ultrathin metasurfaces but also exhibits a new degree of freedom in information transfer between spin and orbital angular momenta of photons.

3.2 Spin-dependent splitting in momentum space

PB phase is the other kind of geometric phase introduced by the spin-orbit interaction of light. As shown above, the cyclic polarization state variation in parameter space will create the spin-dependent geometric PB phase. Thus, if we can spatially design the evolving routes of polarization states on Poincaré sphere, a desired phase distribution can be acquired. In traditional optics, the evolution of polarization can be modulated by a waveplate with a fixed retardation. The orientation of optical axis reference to the incident polarization state $\alpha(x, y)$ and the phase retardation ψ can both be adjusted to change the output state. The state transform in a waveplate can be concluded as

$$\begin{pmatrix} 1 \\ \sigma_{\pm} i \end{pmatrix} \rightarrow \cos\frac{\psi}{2}\begin{pmatrix} 1 \\ \sigma_{\pm} i \end{pmatrix} + i\sin\frac{\psi}{2}\begin{pmatrix} 1 \\ \sigma_{\mp} i \end{pmatrix} e^{i2\sigma\alpha(x,y)}. \tag{5}$$

The above equation indicates that a fraction $\sin^2(\psi/2)$ of the incident photons reverses their handedness and that the other $\cos^2(\psi/2)$ remains unchanged. For the transformed polarization part, ψ and $\alpha(x, y)$ determine the ellipticity and its orientation, respectively. Circular polarizations are the eigenstates of standard Poincaré sphere and essentially corresponded to the orthogonal spin states ($\sigma\pm=\pm1$). As Eq. (5) shows, only the opposite circular polarizations $\sigma_{\mp}$ get the different phase factor $2\sigma\alpha(x, y)$. Hence, the opposite circular polarizations are just considered in the designing of metasurfaces. For $\psi=\pi$, i.e. a half-wave phase retardation, all photons reverse their handedness.

Therefore, the orientation of optical axis of waveplate will restrict the evolving route of polarization state on Poincaré sphere. Figure 10 shows the example of state evolution

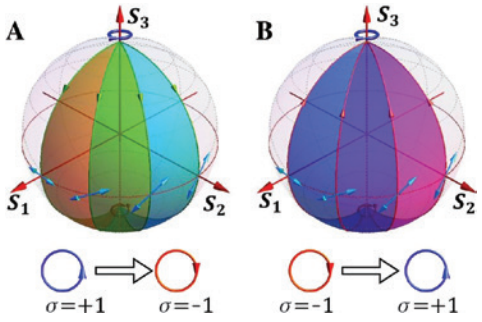

Figure 10: The accumulations of PB phase for the opposite spin components, the left picture (A) shows the transformation from left circular polarization (σ=+1) to right one (σ=-1). Oppositely, the right picture (B) shows the transformation in a different direction. As the reversal of incident polarization, the sense of generated PB phase will be changed.

on Poincaré sphere along different routes and directions. Four different routes following the longitudes are marked with arrow lines; green and red represent the direction toward or backward to the south pole. The blue arrows on the equator are the representations of optical axis orientation. As what we have deduced above, PB phase is equal to half of the solid angle enclosed by the routes on the surface; thus, the induced PB phase would be

$$\mathbf{\Phi}_G = \mathbf{\Phi}_0 + \frac{\sigma\alpha}{2\pi}\cdot 4\pi = \mathbf{\Phi}_0 + 2\sigma\alpha(x, y), \tag{6}$$

where σ is the direction of evolving route. It can be seen that the phase difference $\Delta\mathbf{\Phi}_G = \mathbf{\Phi}_G - \mathbf{\Phi}_0 = 2\sigma\alpha(x, y)$ is in agreement with Eq. (4). By this way, the orientation of local optical axis can be tailored to design the PB phase.

In the above section, the phase gradient in k-space leads to the photonic SHE in the position space. Here, a spin-dependent splitting in k-space will be desired as the PB phase can be tailored by arranging the orientation of local optical axis in position space. A shift of wave vector will arise due to the phase gradient,

$$\Delta k(x, y) = \nabla\mathbf{\Phi}_G(x, y) = \frac{\partial\mathbf{\Phi}_G}{\partial x}\hat{e}_x + \frac{\partial\mathbf{\Phi}_G}{\partial y}\hat{e}_y \tag{7}$$

where $\hat{e}_x$ and $\hat{e}_y$ are the unit direction vectors in x axis and y axis of space coordinate.

Following the above analysis, for circularly polarized light passing through the metasurface with designed local optical axes and the phase retardation of medium set to be π, the spin of incident light beam will be totally reversed and the shift of wave vector can be deduced as

$$\Delta k(x, y) = \Delta k_x + \Delta k_y = 2\sigma\Lambda_x\hat{e}_x + 2\sigma\Lambda_y\hat{e}_y, \tag{8}$$

where $\Lambda_x = \partial\alpha(x, y)/\partial x$ and $\Lambda_x = \partial\alpha(x, y)/\partial y$ are the rotational speed of local optical axes in x and y axes. Moreover, the shift of wave vector in momentum space will cause an angular shift in position space after propagation. For linearly polarized beam, which is the superposition of right circular polarization and left circular polarization, the splitting distance of orthogonal spin components in the observing distance z can be derived as

$$d = 2\left(\frac{\Delta k}{k_0}\right)z. \tag{9}$$

The spin-dependent shift in momentum space has been reported by Shitrit et al. in 2011 [38], where the transmission spectra of coupled localized plasmonic chains are studied. The photonic SHE is observed under the interaction with a curved chain constructed by isotropic unit

cells or with a straight line comprising rotated rectangular cells as shown in Figure 11. Moreover, the plasmonic chains can be changed to modulate the phase front of beam. A wavefront phase dislocation was observed in a circular curvature, in which the dislocation strength was enhanced by the locally anisotropic effect. A vortex with topological charge l=2 is acquired in the spin-flip component when the circular curvature is constructed by the isotropic building blocks, and vortex with topological charge l=4 is observed when the circular curvature is constructed by the arranged anisotropic cells.

Studies on the spin-dependent effect modulated by PB phase have been carried out for several years, and all their results are valuable. However, the observable photonic SHE of propagated light is still a huge topic. Ling et al. reported a giant photonic SHE recently [39]. The gradient metasurface was fabricated by the femtosecond laser self-assembly of nanostructures in fused silica. The rotated local optical axes in horizontal direction endowed the metasurface with a spin-dependent phase gradient. Thus, the angular splitting in position space can be detected directly after the glass. The transparent silica glass promised the high transport efficiency of transmission mode. The polariscopic analysis result and SEM picture are used to describe the inner structure (Figure 12A and B), and Figure 12C–F show the observed intensity and S_3 results. This effect operated at the transmission mode and the Ohmic loss of metallic plasmonic structure is avoided. Based on the PB phase metasurfaces, the direction of spin-dependent splitting can also be modulated by arranging the pattern of local optical axes. Photonic SHE occurring in radial direction and longitudinal direction have been reported lately [109–111].

Another work is devoted to enhance the efficiency of photonic SHE in metallic plasmonic metasurfaces [40]. A certain criterion is developed from the general Jones matrix analysis. Such a criterion is approachable from two different routes, leading to two types of metasurfaces with distinct symmetry properties. While the idea is realizable at general frequencies, as a proof of concept, the fabricated two realistic microwave samples and performed experiments demonstrate that both can realize photonic SHE with ≈90% efficiency within a broad frequency bandwidth. Finally, the experiment demonstrates that the metasurfaces can work as efficiently, and broadband polarization detectors are one illustration of many potential applications of our findings.

Many primary works about the PB phase-caused photonic SHE is focused on the propagating electromagnetic surface waves, where the PB phase gradient will guide the spin-dependent splitting in the metallic interface [24, 48, 59, 112–116]. The collective oscillation of the electrons at the surface of a metal caused by the coupling with light is dubbed as the SPPs. The SPPs can be closely related to the composition and structure of materials and therefore has led to many advances in the control of light at the nanoscale. The photonic SHE involved in this effect may provide a polarization-dependent sensitivity in controlling the directionality of SPPs devices [117, 118]. However, it is

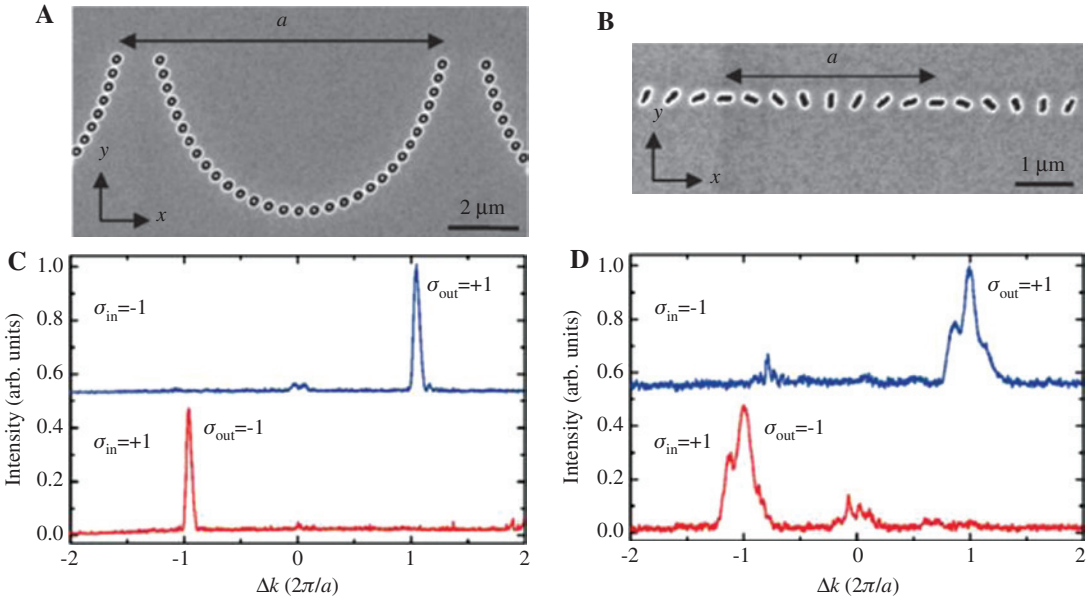

Figure 11: SEM images of a plasmonic chain with identical unit cells but arranged in a curve with period a (A) and another chain with rotated rectangular cells in a straight line (B). (C) and (D) are the spin-dependent momentum deviations for these two different arranged plasmonic chains, respectively. The red and blue lines stand for incident spin states σ=+1, respectively. Adapted from Ref. [38].

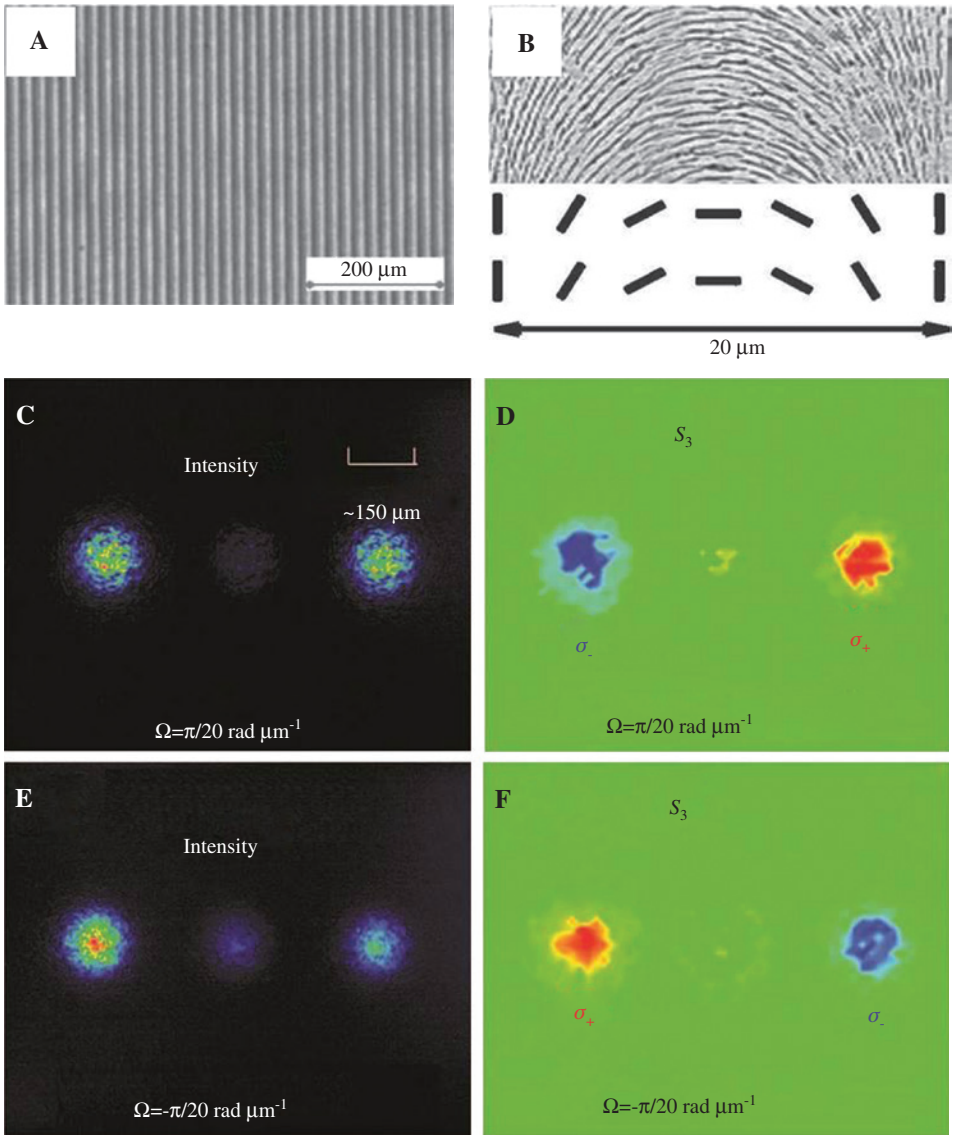

Figure 12: The far field giant photonic SHE observed after a linearly polarized beam passes through two structured metasurfaces. (A) and (B) are the polariscopic analysis result and SEM image picture of the applied metasurface. (C) and (D) show the intensity and S_3 parameter for the metasurface with a rotation rate of $\mathbf{\Omega}=\pi/20$ rad μm^{-1}, respectively. (E) and (F) are the corresponding results for another sample with the exactly opposite rotational rate of $\mathbf{\Omega}=-\pi/20$ rad μm^{-1}. The observation distance is 10 cm away from the metasurface. Adapted from Ref. [39].

substantially different with photonic SHE of light beam; thus, it was not mentioned in this review. Breaking the rotational symmetry of PB phase elements may be the basic requirement for observing the photonic SHE [119, 120], and the rotation rate of local optical axes in metasurfaces is related to magnitude of splitting [38, 121, 122].

4 Photonic spin-Hall devices

Engineering the spin-orbit interaction provides a route to modify the dispersion of an artificial material. Therefore, the spin and orbit can be both selected as a degree of freedom to control the light. The designing of geometric phase enables the spin-based optical devices, which makes the multifunctional spin-dependent element accessible. Moreover, the modulation of PB phase is basically the controlling of light polarization, which is different from the traditional devices based on dynamic phase. In the traditional cases, a phase distribution is designed by adjusting the thickness of optical materials or modulating the reflective indexes. However, the development of integration optics requires the miniaturization and planarization of elements. To develop the infinitesimally

thin and multifunctional devices, the photonic SHE can be designed in cooperation with the functionalities of traditional elements. In this part, we will review the photonic SHE devices that give variety to the primary optical elements.

4.1 Spin-dependent splitter

Polarizing beam splitter can separate the orthogonally polarized components of beam into different propagation directions. A birefringence crystal with considerable thickness is required for the conventional polarizing beam splitter. Therefore, it cannot be integrated in a compact optical system. Particularly, the circular polarization beam splitter is further limited with the absence of natural materials with sufficient circular birefringence [123, 124]. However, spin angular momentum essentially corresponds to the circular polarization of light; thus, the generator of photonic SHE can be instinctively regarded as a circular polarization beam splitter.

As discussed in the earlier section, PB phase gradient can make a photonic SHE with controllable splitting angle in position space, which thus can be treated as a circular polarization beam splitter. However, the intensity pattern of beam is also a major issue for applications in spin-based optical information processing and imaging systems. Figure 13 shows the intensity separation of a modulated light beam [125]. The left column shows intensity patterns generated by a phase-only spatial light modulator. And

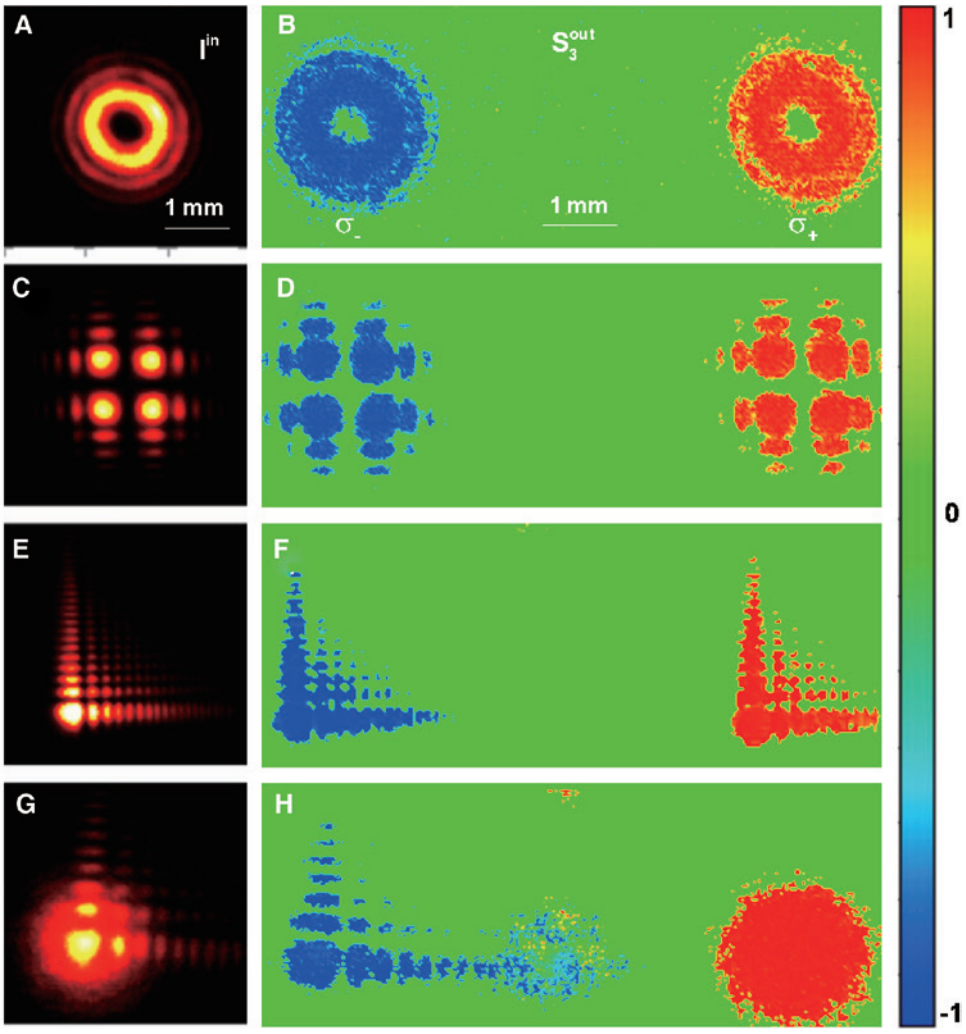

Figure 13: Left column shows the intensity patterns of three typical linear polarization beams (vortex beam, Hermite-Gaussian beam, and Airy beam in the order from top to bottom) and the superposition of a right-handed circular polarization plane Gauss beam and a left-handed circular polarization Airy beam. Right column is the corresponding normalized Stokes parameter S_3 after the spin-dependent splitter. Blue color represents the right polarization and red for left polarization. Adapted from Ref. [125].

the right column shows the splitting results; red and blue represent the orthogonal circular polarizations (σ=±1). The splitter is fabricated by femtosecond laser writing subwavelength grating in a fused silica glass. Thus, a high transmission efficiency, 50.1%, and a high conversion efficiency, 96.3% (note that the transmission losses are not taken into account when evaluating the conversion efficiency), at 632.8 nm wavelength are measured by a laser power meter.

4.2 Pancharatnam-Berry phase lens

As a most frequently used element in optics, a lens is an indispensable part of most optical systems. To make a lightweight and small-volume lens, a variety of schemes have been proposed in the past. Fresnel lens is the most popular solution which introduced a gradual phase gradient in the radial direction to focus light. However, it is still restricted to a thickness comparable to the wavelength (λ_0/n, the effective wavelength in medium), as the requirement of a whole period phase retardation 2π. The development of metasurface offers an efficient way to directly manage the spectral responses of light and thus can be applied to further reduce the thickness of lenses [86, 87, 126, 127]. Moreover, the PB phase elements possess different responses to the orthogonal circularly polarized light [56, 88, 128, 129] and thus will endow the lens novel freedom for light manipulation.

Figure 14 is the PB phase lens proposed by Hasman et al. in 2003 [90]. A discrete structure realized by using the computer-generated space-variant subwavelength dielectric grating is equal to a Fresnel lens. This structure operates at infrared radiation wavelength 10.6 mm. A dielectric lens working in the visible spectrum is reported in 2014 by Lin et al. [58]. These works follow a general strategy to design the PB phase elements. The subwavelength grating features linear phase dependence with the orientation of grating, as shown in Figure 14A; thus, any phase distribution can be accessed by patterning the subwavelength gratings. The phase profile required for a desired optical field can be determined by the Fourier optics. Therefore, by discretizing the phase profile, such a planar lens was obtained in the mentioned works.

Also, the metallic structure can be applied to realize the PB phase lens. Metal is firstly used as the resonance antenna of metasurface, because of the requirement of loss materials whose imaginary part of the complex refractive index is comparable to the real part. However, ohmic losses in the metal and the limited scattering cross sections of the antennas have constrained the efficiency of metasurfaces operating in transmission

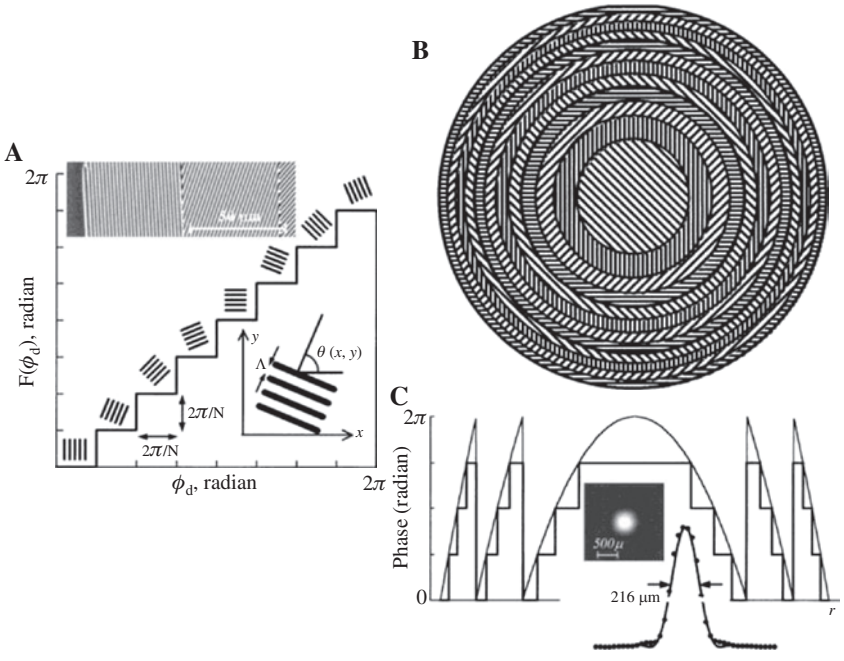

Figure 14: (A) The relationship between the designed phase and the discrete local grating orientation. Inset is the SEM image of a region on the subwavelength structure of the focusing lens. (B) Illustration of a PB phase lens with varying subwavelength structures in the radial direction. (C) The geometric phase distribution and the measured light spot. Inset is the measured (dots) and calculated intensity (solid curve) cross section. Adapted from Ref. [90].

mode. Moreover, It has been theoretically shown that only the transmitted cross polarization wave can acquire the geometric phase change range from 0 to 2π, and the cross-polarization coupling efficiency is fundamentally limited to stay below 25% (with respect to the total incident energy) for ultrathin metasurfaces operating with linearly polarized fields, although the power efficiency of metallic metasurfaces can be increased by making the metasurfaces work at reflection mode or by designing the gap plasmon-based metasurfaces [82, 130–132]. Figure 15 reports an ultrathin linear metasurface lens with maximal cross-polarization transmission efficiency reaching 24.7%, where the thickness is about $\lambda/1000$ (λ is the operating wavelength); only tangential electric currents are supported [129].

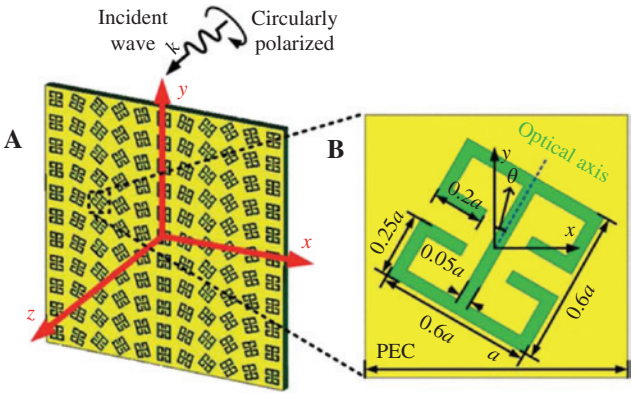

Figure 15: Geometry of the Ding's high efficient metallic metasurface lens. (A) Schematic of the metasurface lens. (B) Geometric parameters of the unit cell. Adapted from Ref. [129].

The spin-related feature of PB phase provides a fresh degree of freedom for light manipulation. Thus, multifunctionality is anticipated in the PB phase lenses. Multifoci diffractive lens has been widely used in various optical systems, which allows a single incident beam to focus at different positions along the longitudinal axis or along the transverse direction. However, the conventional realizations of such a multifoci lens are complex and cumbersome. To miniaturize the multifoci lens and make the focusing controllable, the PB phase-based metasurfaces are applied. Figure 16A shows the schematic metasurface lens with three different focal points along the longitudinal direction [133]. Different polarization states arranged from left to right are listed with linear, right circular, and left circular polarizations. The focused spots are shown in Figure 16B. To realize this function, the metasurface is actually divided into three regions in the radial direction. Different phase profiles are imparted in these regions to focus the different components of linear polarized incident beam, and the focal length is set to be apart. Hence, the position and the polarization of the focal points can be controlled by changing the helicity of the incident light.

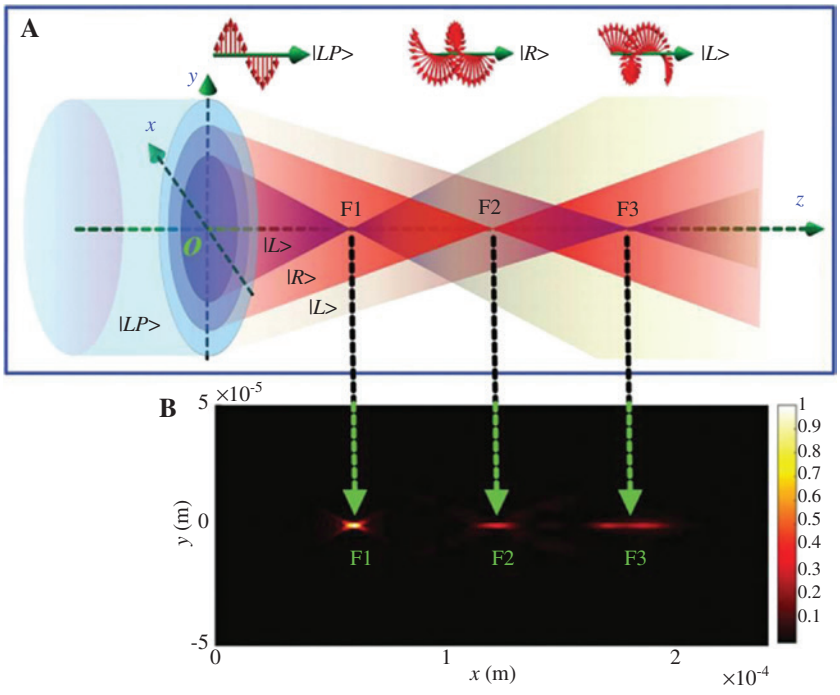

Figure 16: (A) The schematic illustration of the designed longitudinal three-foci metasurface lens; each focal point is the focusing of different polarization components. (B) The observed light spots correspond to the three focal points. Adapted from Ref. [133].

To realize the lens with transverse multifoci, a novel idea is proposed by Wang et al. [134]. Figure 17A is the schematic illustration of the metasurface which is fabricated by etching rectangular slits on a gold film. The substrate is a high-resistance Si wafer. Compared with the design of longitudinal multifoci lens, the antennas are not divided into several distinct regions, but the distribution seems relatively in disorder. This is because the phase profiles supporting the focusing of right and left spin components are simultaneously imprinted on the metasurface. Moreover, to make sure that the two phase profiles are working at the same time, the adjacent slits are working for the different spin components. Therefore, the lens will achieve a giant transverse shift and focus the photons with different spin states to separate spots, when working with a linearly polarized incident beam, as shown in Figure 17B.

4.3 Novel spin-Hall devices

With the development of nanofabrication techniques, a variety of flat devices with more complex and multifunctionality are conceived. The spin-Hall devices based on the PB phase can either work at the linearly polarized incident beams or at a circularly polarized beam but possess distinct responses to the incidences. Apart from the devices developed from the traditional counterparts, such as the polarization beam splitter, laser mode converter [135], and optical lens mentioned above, some novel devices with unprecedented functions are realized. A circular dichroism (CD) spectrometer is an important tool in sensing chiral molecules possessing differential optical responses to circular polarization of light. These molecules are very common in biological and organic compounds. Hence, the CD spectrometer is widely used in biological material studies, protein and DNA structural analysis, and stereochemical detection. Typical CD spectrometers are cumbersome and expensive. Shaltout et al. proposed a novel and integratable CD spectrometer based on the gap-plasmon metasurface with broadband response and one-dimensional phase gradient [132]. The left and right circular polarizations of light are reflected to the opposite directions in position space due to photonic SHE, and the reflection angles for the wavelength components are varied, as shown in Figure 18. Thus, using a broadband detect source, the right and left polarization spectra of samples are obtained in the same time. Additionally, the real-time sensing of chiroptical spectroscopy can also be built in this scheme.

Another spin-Hall device with novel function is the Stokes parameters detector which is proposed by Pors et al. [136]. Polarization is one of the most important features of electromagnetic waves, which is generally characterized by the Stokes parameters (S_0, S_1, S_2, S_3). However, for each of the Stokes parameter, a single measurement is needed in the experiment. Thus, it is not easy to determine the polarization state of beam in real time. Pors et al. carefully designed a metasurface for simultaneous determination of the normalized Stokes parameters. Figure 19 shows the schematic of their Stokes parameters detector. It was realized by interweaving three distinct metasurfaces which can separately probe the normalized Stokes parameters of wave.

To extend the multifunctionality of flat optical devices, Veksler et al. proposed a disorder structure most recently [137]. Apparently, the optical spin provides an additional degree of freedom in the gradient metasurfaces based on the PB phase by breaking the rotational symmetry. However, the unidirectional arrangement of building blocks can only provide a feasible channel for the directional responses. To overcome this disadvantage, the channels arising from the symmetry breaking can be

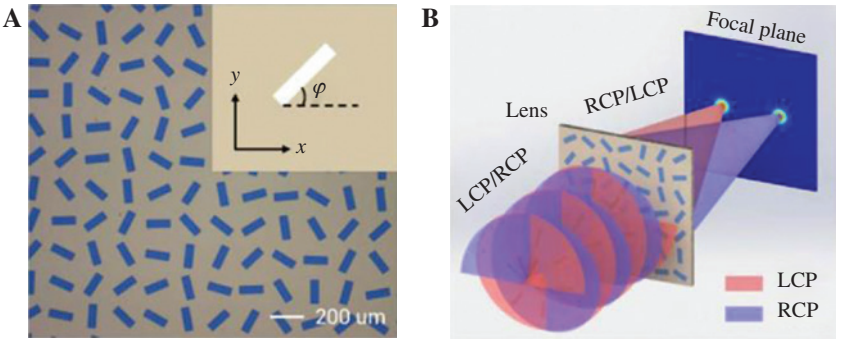

Figure 17: Schematic illustration of the transverse two-foci metasurface lens. (A) The distribution of rectangular silt antennas in metasurface. (B) The metasurface lens focus the incoming beam to two apart spots according to the sense of circular polarization. Adapted from Ref. [134].

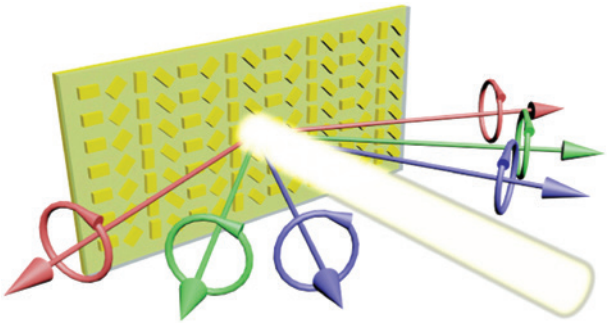

Figure 18: Illustration of a proposed circular dichroism spectrometer. The components with different polarizations are reflected in opposite directions, and each wavelength component is reflected at a different angle. Colors represent the different wavelength values. Adapted from Ref. [132].

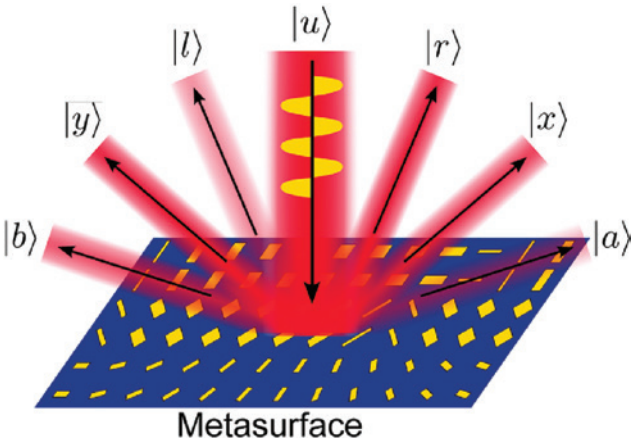

Figure 19: The Stokes parameter detector proposed by Pors et al. $|u\rangle$ is the incoming state with unknown polarization, ($|x\rangle$, $|y\rangle$), ($|a\rangle$, $|b\rangle$), and ($|r\rangle$, $|l\rangle$) can determine the Stokes parameters S_1, S_2, and S_3, respectively. Adapted from Ref. [136].

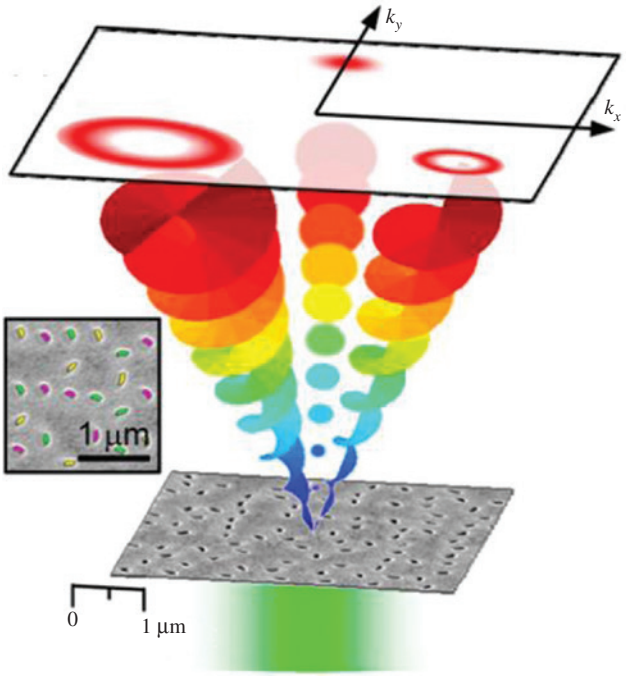

Figure 20: Schematic of spin-controlled far-field phase functions with different orbital angular momenta generated by a disorder gradient metasurface. The inset shows the mixed antenna groups, where each color corresponds to a different wavefront. Adapted from Ref. [137].

increased by constructing a disorder structure. A metasurface with three applicable wavefronts is demonstrated in Figure 20. Light components with different topological charges are deflected to different directions.

5 Conclusions and perspectives

We have presented a brief review on photonic SHE in metasurfaces. The metasurfaces provide an efficient approach to manipulate the spin-orbit interaction, which leads to the photonic SHE. Geometric phase is the result of spin-orbit interaction and at the same time is the reason of spin-dependent responses in light-matter interaction. Two kinds of geometric phases (spin-redirection phase and PB phase) are involved in the explanation of spin-dependent splitting in the photonic SHE. The first one is related to the change of the propagation direction of light. When a light beam propagates in a curved trajectory, the transversality of electromagnetic waves will require a geometric rotation of the polarization; therefore, an induced geometric spin-redirection phase serving as the back-action of the polarization variation will lead to the splitting of spin photons in position space. The PB phase is related to polarization evolution. Different polarization-evolving routes on Stokes parameter space will impart the wave a corresponding phase change. By appropriately tailoring the polarization, a geometric phase gradient will cause the spin-dependent splitting of photons in momentum space. This splitting is expressed as an angular deviation in the position space, and the splitting angle can be changed by altering the PB phase gradient. For this reason, the space shift induced by the PB phase will increase with the propagation distance.

Metasurface is an artificial material with excellent flexibility in controlling light beam. An infinitesimal dimension of the metasurfaces makes them efficient and integratable with other planar devices. Because of the subwavelength-scale building blocks and their

separations, the response of metasurfaces is determined by the structure rather than the material. Therefore, the features of light can be locally molded by a metasurface based on subwavelength structures. The spin-orbit interaction can also be modulated in the metasurface by changing the propagation trajectory or by directly tailoring the local polarization. As mentioned already, two different kinds of splitting results of spin photons will be created by these modulations. Consequently, metasurfaces provide a convenient way to enhance the originally very weak photonic SHE, and then the manipulation of this effect is realized.

The photonic spin-Hall devices are based on the modulation of photonic SHE in metasurfaces. Spin provides an additional degree of freedom for these devices. Therefore, by appropriately designing the metasurfaces, not only the functions of conventional optical devices are realized by the metasurfaces, but also some unprecedented functions are found, for example, the spin-related multifoci lens. Moreover, photonic SHE enables the realization of multifunctionality in single metasurfaces, which means that the response of spin-Hall devices can be adjusted by changing the incident polarization. Great flexibility and multifunctionality are uncovered by the combination of photonic SHE and metasurfaces.

In the future, the researches and applications of photonic SHE will be pushed forward with the continuous development of metasurfaces. The search of highly efficient and reconfigurable materials for metasurfaces will no doubt promote the performance and enable the new functionalities of spin-Hall devices. The external conditions such as the voltage, temperature, light, and the magnetic field can be used to change the refractive index, geometric pattern, and arrangement of the building blocks. Thus, the multifunctionality of spin-Hall devices can be significantly enhanced, such as the existing researches in liquid crystal PB elements. Furthermore, compact and tunable optical devices will be realized by integrating metasurfaces. The modulation of light in metasurfaces occurs at a subwavelength scale off the surface, which approximates the infinitesimal dimension of 2D metasurfaces, thus allowing metasurfaces to be stacked as a whole. The combination with photonic SHE and the employment of reconfigurable materials enable the flexible real-time controlling of light flow. All of these features make it possible to obtain the compact optical devices with a high tunability. Moreover, the design of metasurfaces enables direct observation of the photonic SHE and enables the applications of photonic SHE by controlling the spin-orbit interaction. However, the degree of freedom associated with orbital angular momentum is seldom referred to in the existing metasurfaces. Different from the spin angular momentum which is restricted to two eigenstates, the orbital angular momentum have an infinite number of eigenstates. Thus, the applications of the eigenstates of orbital angular momentum may dramatically increase the channels for information transfer and the freedom for light manipulation.

Acknowledgments: This research was supported by the National Natural Science Foundation of China (Grant Nos. 11274106 and 11474089).

References

[1] Onoda M, Murakami S, Nagaosa N. Hall effect of light. Phys Rev Lett 2004;93:083901.
[2] Bliokh KY, Bliokh YP. Conservation of angular momentum, transverse shift, and spin Hall effect in reflection and refraction of an electromagnetic wave packet. Phys Rev Lett 2006;96:073903.
[3] Wolf SA, Awschalom DD, Buhrman RA, Daughton JM, von Molnár S, Roukes ML, Chtchelkanova AY, Treger DM. Spintronics: a spin-based electronics vision for the future. Science 2001;294:1488–95.
[4] Awschalom DD, Flatté ME. Challenges for semiconductor spintronics. Nat Phys 2007;3:153–9.
[5] Chappert C, Fert A, Van Dau FN. The emergence of spin electronics in data storage. Nat Mater 2007;6:813–23.
[6] Wunderlich J, Park BG, Irvine AC, Zârbo LP, Rozkotová E, Nemec P, Novák V, Sinova J, Jungwirth T. Spin Hall effect transistor. Science 2010;330:1801–4.
[7] Aharonov Y, Albert DZ, Vaidman L. How the result of a measurement of a component of the spin of a spin-1/2 particle can turn out to be 100. Phys Rev Lett 1988;60:1351–4.
[8] Hosten O, Kwiat P. Observation of the spin hall effect of light via weak measurements. Science 2008;319:787–90.
[9] Qin Y, Li Y, He H, Gong Q. Measurement of spin Hall effect of reflected light. Opt Lett 2009;34:2551–3.
[10] Zhou X, Xiao Z, Luo H, Wen S. Experimental observation of the spin Hall effect of light on a nanometal film via weak measurements. Phys Rev A 2012;85:043809.
[11] Zhou X, Ling X, Luo H, Wen S. Identifying graphene layers via spin Hall effect of light. Appl Phys Lett 2012;101:251602.
[12] Zhou X, Zhang J, Ling X, Chen S, Luo H, Wen S. Photonic spin Hall effect in topological insulators. Phys Rev A 2013;88:053840.
[13] Ringel Z. Using weak measurements to extract the Z_2 index of a topological insulator. Phys Rev B 2015;91:241109.
[14] Li D, Shen Z, He Y, Zhang Y, Chen Z, Ma H. Application of quantum weak measurement for glucose concentration detection. Appl Opt 2016;55:1697–702.
[15] Bliokh KY, Niv A, Kleiner V, Hasman E. Geometrodynamics of spinning light. Nat Photon 2008;2:748–53.
[16] Luo H, Zhou X, Shu W, Wen S, Fan D. Enhanced and switchable spin Hall effect of light near the Brewster angle on reflection. Phys Rev A 2011;84:043806.

[17] Kong LJ, Wang XL, Li SM, Li YN, Chen J, Gu B, Wang HT. Spin Hall effect of reflected light from an air-glass interface around the Brewster's angle. Appl Phys Lett 2012;100:071109.
[18] Ling XH, Luo HL, Tang M, Wen SC. Enhanced and tunable spin Hall effect of light upon reflection of one-dimensional photonic crystal with a defect layer. Chin Phys Lett 2012;29:074209.
[19] Roy B, Ghosh N, Banerjee A, Gupta SD, Roy S. Manifestations of geometric phase and enhanced spin Hall shifts in an optical trap. New J Phys 2014;16:083037.
[20] Wang B, Li Y, Pan MM, Ren JL, Xiao YF, Yang H, Gong Q. Measuring spin Hall effect of light by cross-polarization intensity ratio. Opt Lett 2014;39:3425–8.
[21] Kildishev AV, Boltasseva A, Shalaev VM. Planar photonics with metasurfaces. Science 2013;339:1232009.
[22] Yin X, Ye Z, Rho J, Wang Y, Zhang X. Photonic spin Hall effect at metasurfaces. Science 2013;339:1405–7.
[23] Yu N, Genevet P, Kats MA, Aieta F, Tetienne JP, Capasso F, Gaburro Z. Light propagation with phase discontinuities: generalized laws of reflection and refraction. Science 2011;334:333–7.
[24] Huang L, Chen X, Bai B, Tan Q, Jin G, Zentgraf T, Zhang S. Helicity dependent directional surface plasmon polariton excitation using a metasurface with interfacial phase discontinuity. Light Sci Appl 2013;2:e70.
[25] Lin J, Mueller JP, Wang Q, Yuan G, Antoniou N, Yuan XC, Capasso F. Polarization-controlled tunable directional coupling of surface plasmon polaritons. Science 2013;340:331–4.
[26] Shitrit N, Yulevich I, Maguid E, Ozeri D, Veksler D, Kleiner V, Hasman E. Spin-optical metamaterial route to spin-controlled photonics. Science 2013;340:724–6.
[27] Yu N, Capasso F. Flat optics with designer metasurfaces. Nat Mater 2014;13:139–50.
[28] Zhao Y, Liu XX, Alù A. Recent advances on optical metasurfaces. J Opt 2014;16:123001.
[29] Meinzer N, Barnes WL, Hooper IR. Plasmonic meta-atoms and metasurfaces. Nat Photon 2014;8:889–98.
[30] Aieta F, Genevet P, Yu N, Kats MA, Gaburro Z, Capasso F. Out-of-plane reflection and refraction of light by anisotropic optical antenna metasurfaces with phase discontinuities. Nano Lett 2012;12:1702–6.
[31] Genevet P, Yu N, Aieta F, Lin J, Kats MA, Blanchard R, Scully MO, Gaburro Z, Capasso F. Ultra-thin plasmonic optical vortex plate based on phase discontinuities. Appl Phys Lett 2012;100:013101.
[32] Blanchard R, Aoust G, Genevet P, Yu N, Kats MA, Gaburro Z, Capasso F. Modeling nanoscale V-shaped antennas for the design of optical phased arrays. Phys Rev B 2012;85:155457.
[33] Larouche S, Smith DR. Reconciliation of generalized refraction with diffraction theory. Opt Lett 2012;37:2391–3.
[34] Zhao Y, Alù A. Tailoring the dispersion of plasmonic nanorods to realize broadband optical meta-waveplates. Nano Lett 2013;13:1086–91.
[35] Shaltout A, Liu J, Shalaev VM, Kildishev AV. Optically active metasurface with non-chiral plasmonic nanoantennas. Nano Lett 2014;14:4426–31.
[36] Wang S, Abeysinghe DC, Zhan Q. Generation of vectorial optical fields with slot-antenna-based metasurface. Opt Lett 2015;40:4711–4.
[37] Pu M, Chen P, Wang Y, Zhao Z, Huang C, Wang C, Ma X, Luo X. Anisotropic meta-mirror for achromatic electromagnetic polarization manipulation. Appl Phys Lett 2013;102:131906.
[38] Shitrit N, Bretner I, Gorodetski Y, Kleiner V, Hasman E. Optical spin Hall effects in plasmonic chains. Nano Lett 2011;11:2038–42.
[39] Ling X, Zhou X, Yi X, Shu W, Liu Y, Chen S, Luo H, Wen S, Fan D. Giant photonic spin Hall effect in momentum space in a structured metamaterial with spatially varying birefringence. Light Sci Appl 2015;4:e290.
[40] Luo W, Xiao S, He Q, Sun S, Zhou L. Photonic spin Hall effect with nearly 100% efficiency. Adv Opt Mater 2015;3:1102–8.
[41] Bliokh KY, Nori F. Transverse and longitudinal angular momenta of light. Phys Rep 2015;592:1–38.
[42] Beth RA. Mechanical detection and measurement of the angular momentum of light. Phys Rev 1936;50:115–25.
[43] Humblet J. Sur le moment d'impulsion d'une onde électromagnétique. Physica 1943;10:585–603.
[44] Allen L, Beijersbergen MW, Spreeuw RJ, Woerdman JP. Orbital angular momentum of light and the transformation of Laguerre-Gaussian laser modes. Phys Rev A 1992;45:8185–9.
[45] Mathur H. Thomas precession, spin-orbit interaction, and Berry's phase. Phys Rev Lett 1991;67:3325–7.
[46] Liberman VS, Zel'dovich BY. Spin-orbit interaction of a photon in an inhomogeneous medium. Phys Rev A 1992;46:5199–207.
[47] Niv A, Gorodetski Y, Kleiner V, Hasman E. Topological spin-orbit interaction of light in anisotropic inhomogeneous subwavelength structures. Opt Lett 2008;33:2910–2.
[48] O'Connor D, Ginzburg P, Rodríguez-Fortuño FJ, Wurtz GA, Zayats AV. Spin-orbit coupling in surface plasmon scattering by nanostructures. Nat Commun 2014;5:5327.
[49] Bliokh KY, Rodríguez-Fortuño FJ, Nori F, Zayats AV. Spin–orbit interactions of light. Nat Photon 2015;9:796–808.
[50] O'Neil AT, MacVicar I, Allen L, Padgett MJ. Intrinsic and extrinsic nature of the orbital angular momentum of a light beam. Phys Rev Lett 2002;88:053601.
[51] Allen L, Padgett MJ, Babiker M. The orbital angular momentum of light. Prog Opt 1999;39:291–372.
[52] Vinitskiĭ S, Derbov V, Dubovik V, Markovski B, Stepanovskiĭ Y. Topological phases in quantum mechanics and polarization optics. Soviet Physics Uspekhi 1990;33:403–28.
[53] Bhandari R. Polarization of light and topological phases. Phys Rep 1997;281:1–64.
[54] Bomzon Z, Kleiner V, Hasman E. Computer-generated space-variant polarization elements with subwavelength metal stripes. Opt Lett 2001;26:33–5.
[55] Bomzon Z, Biener G, Kleiner V, Hasman E. Space-variant Pancharatnam-Berry phase optical elements with computer-generated subwavelength gratings. Opt Lett 2002;27:1141–3.
[56] Papakostas A, Potts A, Bagnall DM, Prosvirnin SL, Coles HJ, Zheludev NI. Optical manifestations of planar chirality. Phys Rev Lett 2003;90:107404.
[57] Huang L, Chen X, Mühlenbernd H, Li G, Bai B, Tan Q, Jin G, Zentgraf T, Zhang S. Dispersionless phase discontinuities for controlling light propagation. Nano Lett 2012;12:5750–5.
[58] Lin D, Fan P, Hasman E, Brongersma ML. Dielectric gradient metasurface optical elements. Science 2014;345:298–302.
[59] Bliokh KY, Gorodetski Y, Kleiner V, Hasman E. Coriolis effect in optics: unified geometric phase and spin-Hall effect. Phys Rev Lett 2008;101:030404.

[60] Bliokh KY. Geometrodynamics of polarized light: Berry phase and spin Hall effect in a gradient-index medium. J Opt A: Pure Appl Opt 2009;11:094009.
[61] Rytov S. On the transition from wave to geometrical optics. Dokl Akad Nauk SSSR 1938;18:263–7.
[62] Vladimirskii V. The rotation of a polarization plane for curved light ray. Dokl Akad Nauk SSSR 1941;21:222–5.
[63] Berry MV. Quantal phase factors accompanying adiabatic changes. Proc R Soc London Ser A 1984;392:45–57.
[64] Pancharatnam S. Generalized theory of interference, and its applications. Part I. Coherent pencils. Proc Indian Acad Sci A 1956;44:398–417.
[65] Berry MV. The adiabatic phase and Pancharatnam's phase for polarized light. J Mod Opt 1987;34:1401–7.
[66] Simon R, Kimble HJ, Sudarshan EC. Evolving geometric phase and its dynamical manifestation as a frequency shift: An optical experiment. Phys Rev Lett 1988;61:19–22.
[67] Bhandari R, Samuel J. Observation of topological phase by use of a laser interferometer. Phys Rev Lett 1988;60:1211–3.
[68] Poincaré H. Leçons sur la théorie mathématique de la lumière., Théorie mathématique de la lumière. II, Nouvelles études sur la diffraction, théorie de la dispersion de Helmholtz: leçons professées pendant le premier semestre 1891-1892/par H. Poincaré,...; rédigées par M. Lamotte et D. Hurmuzescu 1892.
[69] Milione G, Sztul HI, Nolan DA, Alfano RR. Higher-order Poincare sphere, stokes parameters, and the angular momentum of light. Phys Rev Lett 2011;107:053601.
[70] Milione G, Evans S, Nolan DA, Alfano RR. Higher order Pancharatnam-Berry phase and the angular momentum of light. Phys Rev Lett 2012;108:190401.
[71] Holleczek A, Aiello A, Gabriel C, Marquardt C, Leuchs G. Classical and quantum properties of cylindrically polarized states of light. Opt Express 2011;19:9714–36.
[72] Yi X, Liu Y, Ling X, Zhou X, Ke Y, Luo H, Wen S, Fan D. Hybrid-order Poincaré sphere. Phys Rev A 2015;91:023801.
[73] Pendry JB, Schurig D, Smith DR. Controlling electromagnetic fields. Science 2006;312:1780–2.
[74] Leonhardt U. Optical conformal mapping. Science 2006;312:1777–80.
[75] Brorson SD, Haus HA. Diffraction gratings and geometrical optics. J Opt Soc Am B 1988;5:247–8.
[76] Feynman R, Hibbs A. Quantum Mechanics and Path Integrals. New York: McGraw-Hill, 1965.
[77] Hecht E. Optics. 3rd edn. Boston: Addison Wesley, 1997.
[78] Sun S, Yang KY, Wang CM, Juan TK, Chen WT, Liao CY, He Q, Xiao S, Kung WT, Guo GY, Zhou L, Tsai DP. High-efficiency broadband anomalous reflection by gradient meta-surfaces. Nano Lett 2012;12:6223–9.
[79] Sun S, He Q, Xiao S, Xu Q, Li X, Zhou L. Gradient-index meta-surfaces as a bridge linking propagating waves and surface waves. Nat Mater 2012;11:426–31.
[80] Huang L, Chen X, Mühlenbernd H, Zhang H, Chen S, Bai B, Tan Q, Jin G, Cheah KW, Qiu CW, Li J, Zentgraf T, Zhang S. Three-dimensional optical holography using a plasmonic metasurface. Nat Commun 2013;4:2808.
[81] Yang Y, Wang W, Moitra P, Kravchenko, II, Briggs DP, Valentine J. Dielectric meta-reflectarray for broadband linear polarization conversion and optical vortex generation. Nano Lett 2014;14:1394–9.
[82] Li Z, Palacios E, Butun S, Aydin K. Visible-frequency metasurfaces for broadband anomalous reflection and high-efficiency spectrum splitting. Nano Lett 2015;15:1615–21.
[83] Yu N, Aieta F, Genevet P, Kats MA, Gaburro Z, Capasso F. A broadband, background-free quarter-wave plate based on plasmonic metasurfaces. Nano Lett 2012;12:6328–33.
[84] Kats MA, Genevet P, Aoust G, Yu N, Blanchard R, Aieta F, Gaburro Z, Capasso F. Giant birefringence in optical antenna arrays with widely tailorable optical anisotropy. Proc Natl Acad Sci USA 2012;109:12364–8.
[85] Ni X, Emani NK, Kildishev AV, Boltasseva A, Shalaev VM. Broadband light bending with plasmonic nanoantennas. Science 2012;335:427.
[86] Aieta F, Genevet P, Kats MA, Yu N, Blanchard R, Gaburro Z, Capasso F. Aberration-free ultrathin flat lenses and axicons at telecom wavelengths based on plasmonic metasurfaces. Nano Lett 2012;12:4932–6.
[87] Ni X, Kildishev AV, Shalaev VM. Metasurface holograms for visible light. Nat Commun 2013;4:2807.
[88] Ni X, Ishii S, Kildishev AV, Shalaev VM. Ultra-thin, planar, Babinet-inverted plasmonic metalenses. Light Sci Appl 2013;2:e72.
[89] Biener G, Niv A, Kleiner V, Hasman E. Formation of helical beams by use of Pancharatnam-Berry phase optical elements. Opt Lett 2002;27:1875–7.
[90] Hasman E, Kleiner V, Biener G, Niv A. Polarization dependent focusing lens by use of quantized Pancharatnam-Berry phase diffractive optics. Appl Phys Lett 2003;82:328–30.
[91] Hasman E, Biener G, Niv A, Kleiner V. Space-variant polarization manipulation. Prog Opt 2005;47:215–89.
[92] Marrucci L, Karimi E, Slussarenko S, Piccirillo B, Santamato E, Nagali E, Sciarrino F. Spin-to-orbital conversion of the angular momentum of light and its classical and quantum applications. J Opt 2011;13:064001.
[93] Kang M, Chen J, Wang XL, Wang HT. Twisted vector field from an inhomogeneous and anisotropic metamaterial. J Opt Soc Am B 2012;29:572–6.
[94] Chen X, Huang L, Muhlenbernd H, Li G, Bai B, Tan Q, Jin G, Qiu CW, Zhang S, Zentgraf T. Dual-polarity plasmonic metalens for visible light. Nat Commun 2012;3:1198.
[95] Li G, Kang M, Chen S, Zhang S, Pun EY, Cheah KW, Li J. Spin-enabled plasmonic metasurfaces for manipulating orbital angular momentum of light. Nano Lett 2013;13:4148–51.
[96] Liu Y, Ling X, Yi X, Zhou X, Luo H, Wen S. Realization of polarization evolution on higher-order Poincaré sphere with metasurface. Appl Phys Lett 2014;104:191110.
[97] Pu M, Li X, Ma X, Wang Y, Zhao Z, Wang C, Hu C, Gao P, Huang C, Ren H, Li X, Qin F, Yang J, Gu M, Hong M, Luo X. Catenary optics for achromatic generation of perfect optical angular momentum. Sci Adv 2015;1:e1500396.
[98] Zhang X, Jin J, Wang Y, Pu M, Li X, Zhao Z, Gao P, Wang C, Luo X. Metasurface-based broadband hologram with high tolerance to fabrication errors. Sci Rep 2016;6:19856.
[99] Hall EH. On a new action of the magnet on electric currents. Am J Math 1879;2:287–92.
[100] Hirsch JE. Spin Hall effect. Phys Rev Lett 1999;83:1834–7.
[101] Kato YK, Myers RC, Gossard AC, Awschalom DD. Observation of the spin Hall effect in semiconductors. Science 2004;306:1910–3.

[102] Sinova J, Culcer D, Niu Q, Sinitsyn NA, Jungwirth T, MacDonald AH. Universal intrinsic spin Hall effect. Phys Rev Lett 2004;92:126603.
[103] Wunderlich J, Kaestner B, Sinova J, Jungwirth T. Experimental observation of the spin-Hall effect in a two-dimensional spin-orbit coupled semiconductor system. Phys Rev Lett 2005;94:047204.
[104] Bliokh KY, Bliokh YP. Polarization, transverse shifts, and angular momentum conservation laws in partial reflection and refraction of an electromagnetic wave packet. Phys Rev E 2007;75:066609.
[105] Zhang Y, Li P, Liu S, Zhao J. Unveiling the photonic spin Hall effect of freely propagating fan-shaped cylindrical vector vortex beams. Opt Lett 2015;40:4444–7.
[106] Ling X, Yi X, Zhou X, Liu Y, Shu W, Luo H, Wen S. Realization of tunable spin-dependent splitting in intrinsic photonic spin Hall effect. Appl Phys Lett 2014;105:151101.
[107] Korger J, Aiello A, Chille V, Banzer P, Wittmann C, Lindlein N, Marquardt C, Leuchs G. Observation of the geometric spin Hall effect of light. Phys Rev Lett 2014;112:113902.
[108] Luo H, Ling X, Zhou X, Shu W, Wen S, Fan D. Enhancing or suppressing the spin Hall effect of light in layered nanostructures. Phys Rev A 2011;84:033801.
[109] Li Y, Liu Y, Ling X, Yi X, Zhou X, Ke Y, Luo H, Wen S, Fan D. Observation of photonic spin Hall effect with phase singularity at dielectric metasurfaces. Opt Express 2015;23:1767–74.
[110] Shu W, Ke Y, Liu Y, Ling X, Luo H, Yin X. Radial spin Hall effect of light. Phys Rev A 2016;93:013839.
[111] Liu S, Li P, Zhang Y, Gan X, Wang M, Zhao J. Longitudinal spin separation of light and its performance in three-dimensionally controllable spin-dependent focal shift. Sci Rep 2016;6:20774.
[112] Gorodetski Y, Shitrit N, Bretner I, Kleiner V, Hasman E. Observation of optical spin symmetry breaking in nanoapertures. Nano Lett 2009;9:3016–9.
[113] Liu Y, Zhang X. Metasurfaces for manipulating surface plasmons. Appl Phys Lett 2013;103:141101.
[114] Pors A, Nielsen MG, Bernardin T, Weeber JC, Bozhevolnyi SI. Efficient unidirectional polarization-controlled excitation of surface plasmon polaritons. Light Sci Appl 2014;3:e197.
[115] Kapitanova PV, Ginzburg P, Rodríguez-Fortuño FJ, Filonov DS, Voroshilov PM, Belov PA, Poddubny AN, Kivshar YS, Wurtz GA, Zayats AV. Photonic spin Hall effect in hyperbolic metamaterials for polarization-controlled routing of subwavelength modes. Nat Commun 2014;5:3226.
[116] Xiao S, Zhong F, Liu H, Zhu S, Li J. Flexible coherent control of plasmonic spin-Hall effect. Nat Commun 2015;6:8360.
[117] Kavokin A, Malpuech G, Glazov M. Optical spin hall effect. Phys Rev Lett 2005;95:136601.
[118] Leyder C, Romanelli M, Karr JP, Giacobino E, Liew TCH, Glazov MM, Kavokin AV, Malpuech G, Bramati A. Observation of the optical spin Hall effect. Nat Phys 2007;3:628–31.
[119] Ling X, Zhou X, Shu W, Luo H, Wen S. Realization of tunable photonic spin Hall effect by tailoring the Pancharatnam-berry phase. Sci Rep 2014;4:5557.
[120] Liu Y, Ling X, Yi X, Zhou X, Chen S, Ke Y, Luo H, Wen S. Photonic spin Hall effect in dielectric metasurfaces with rotational symmetry breaking. Opt Lett 2015;40:756–9.
[121] Liu Y, Ke Y, Zhou J, Luo H, Wen S. Manipulating the spin-dependent splitting by geometric Doppler effect. Opt Express 2015;23:16682–92.
[122] Liu YC, Chen SZ, Ke YG, Zhou XX, Luo HL, Wen SC. Spin photonics and spin-photonic devices with dielectric metasurfaces. Proc of SPIE 2015;9551:95511Z.
[123] Hasman E, Bomzon Z, Niv A, Biener G, Kleiner V. Polarization beam-splitters and optical switches based on space-variant computer-generated subwavelength quasi-periodic structures. Opt Commun 2002;209:45–54.
[124] Khorasaninejad M, Crozier KB. Silicon nanofin grating as a miniature chirality-distinguishing beam-splitter. Nat Commun 2014;5:5386.
[125] Ke Y, Liu Y, He Y, Zhou J, Luo H, Wen S. Realization of spin-dependent splitting with arbitrary intensity patterns based on all-dielectric metasurfaces. Appl Phys Lett 2015;107:041107.
[126] Aieta F, Genevet P, Kats M, Capasso F. Aberrations of flat lenses and aplanatic metasurfaces. Opt Express 2013;21:31530–9.
[127] Tang D, Wang C, Zhao Z, Wang Y, Pu M, Li X, Gao P, Luo X. Ultrabroadband superoscillatory lens composed by plasmonic metasurfaces for subdiffraction light focusing. Laser Photonics Rev 2015;9:713–9.
[128] Gao K, Cheng HH, Bhowmik AK, Bos PJ. Thin-film Pancharatnam lens with low f-number and high quality. Opt Express 2015;23:26086–94.
[129] Ding X, Monticone F, Zhang K, Zhang L, Gao D, Burokur SN, de Lustrac A, Wu Q, Qiu CW, Alù A. Ultrathin pancharatnam-berry metasurface with maximal cross-polarization efficiency. Adv Mater 2015;27:1195–200.
[130] Pors A, Albrektsen O, Radko IP, Bozhevolnyi SI. Gap plasmon-based metasurfaces for total control of reflected light. Sci Rep 2013;3:2155.
[131] Zheng G, Mühlenbernd H, Kenney M, Li G, Zentgraf T, Zhang S. Metasurface holograms reaching 80% efficiency. Nat Nanotechnol 2015;10:308–12.
[132] Shaltout A, Liu J, Kildishev A, Shalaev V. Photonic spin Hall effect in gap–plasmon metasurfaces for on-chip chiroptical spectroscopy. Optica 2015;2:860–3.
[133] Chen X, Chen M, Mehmood MQ, Wen D, Yue F, Qiu CW, Zhang S. Longitudinal multifoci metalens for circularly polarized light. Adv Opt Mater 2015;3:1201–6.
[134] Wang S, Wang X, Kan Q, Ye J, Feng S, Sun W, Han P, Qu S, Zhang Y. Spin-selected focusing and imaging based on metasurface lens. Opt Express 2015;23:26434–41.
[135] He Y, Liu Z, Liu Y, Zhou J, Ke Y, Luo H, Wen S. Higher-order laser mode converters with dielectric metasurfaces. Opt Lett 2015;40:5506–9.
[136] Pors A, Nielsen MG, Bozhevolnyi SI. Plasmonic metagratings for simultaneous determination of Stokes parameters. Optica 2015;2:716–23.
[137] Veksler D, Maguid E, Shitrit N, Ozeri D, Kleiner V, Hasman E. Multiple wavefront shaping by metasurface based on mixed random antenna groups. ACS Photonics 2015;2:661–7.